JAAS

Accepted Manuscript

This is an *Accepted Manuscript*, which has been through the Royal Society of Chemistry peer review process and has been accepted for publication.

Accepted Manuscripts are published online shortly after acceptance, before technical editing, formatting and proof reading. Using this free service, authors can make their results available to the community, in citable form, before we publish the edited article. We will replace this *Accepted Manuscript* with the edited and formatted *Advance Article* as soon as it is available.

You can find more information about *Accepted Manuscripts* in the Information for Authors.

Please note that technical editing may introduce minor changes to the text and/or graphics, which may alter content. The journal's standard Terms & Conditions and the Ethical guidelines still apply. In no event shall the Royal Society of Chemistry be held responsible for any errors or omissions in this *Accepted Manuscript* or any consequences arising from the use of any information it contains.

ROYAL SOCIETY OF CHEMISTRY

www.rsc.org/jaas

Journal Name

RSCPublishing

ARTICLE

In-situ time-lapse synchrotron radiation X-ray diffraction of silver corrosion

Cite this: DOI: 10.1039/x0xx00000x

Rita Wiesinger[a], Rosie Grayburn[b,c], Mark Dowsett[c], Pieter-Jan Sabbe[b], Paul Thompson[d], Annemie Adriaens[b] and Manfred Schreiner[a]

Received 00th January 2012,
Accepted 00th January 2012

DOI: 10.1039/x0xx00000x

www.rsc.org/

Several heritage systems have been studied using state-of-the-art synchrotron techniques. The cultural heritage value of silver is documented in museum collections across the globe. However, the silver surface is not as chemically stable as that of other precious metals, and is susceptible to corrosion by atmospheric gases. It is therefore of special interest to clarify these surface reactions by using in-situ, time-lapse chemical and structural analysis in controlled ambients in order to develop strategies to reduce or even prevent the atmospheric attacks. In order to study the initial corrosion processes of silver in the presence of corrosive gases in-situ time-lapse X-ray diffraction experiments were performed on the XMaS beamline at the European Synchrotron Radiation Facility, Grenoble. Highly pure silver samples were weathered with synthetic air containing 500 ppb of both H_2S and ozone, at relative humidity (RH) levels, and XRD patterns were tracked every 10 min over a total weathering time of 24h. The time-lapse Synchrotron Radiation (SR)-XRD data show that pure silver exposed to those atmospheres starts to form crystalline corrosion products after only 10 minutes. Silver sulfates, silver oxides, intermediates and mixed species are formed on the sample surface over the duration of the experiment. The data collected using a newly combined environmental cell/gas flow set up introduces a set of highly useful tools for scientists who wish to study time-lapse gaseous corrosion at ambient temperature and pressure.

1. Introduction

Silver and its alloys have been an important part of human technology and art for between 8 and 10 millennia. The metal has had a profound influence on the evolution of human societies. It was venerated in ancient Egypt and valued above gold; it has been used in medicine for its antibacterial properties since at least the 8th Century; it has been used in coins for nearly 3 millennia, and forms a significant part of our cultural heritage in statues, ornaments, jewellery, high-value utensils, currency coins and silverware. Today, silver is extensively used in electronics and electronic devices, metallurgy, sensors, optical devices and artworks. Unfortunately, the chemical stability of silver and its alloys is not as high as of gold, and in storage, operation or display the function as well as the beauty of silver artefacts can be affected or even destroyed by the interaction of their surfaces with the ambient. Conventional atmospheric parameters that affect silver comprise weathering factors (temperature, moisture, radiation, wind velocity etc.), air pollutants (H_2S, SO_2, CO_2, NO_x etc.) and aerosols[1-7]. The degradation caused by an increasing concentration of corrosive gases such as H_2S, SO_2, CO_2 and O_3 of anthropogenic origin and mainly present in urban environment atmospheres is a major challenge to the survival of art objects and other artefacts in museums, private collections or archaeological findings[1, 2, 4, 5, 8-15]. A fundamental understanding of the chemistry occurring on the surfaces is needed in order to be able to control material degradation. As the first hours to days of a cleaned/fresh metal surface exposed to certain atmospheres decide the main corrosion process which then proceeds at different corrosion rates for years it is especially interesting to study those early stages of atmospheric corrosion[1, 2, 16, 17]. This highlights the need to study the reactions occurring in-situ in a controlled environment using time-lapse methods in order to develop strategies to reduce or prevent atmospheric corrosion[15, 18-20].

In the field of heritage science the main cause of silver tarnishing was always attributed to sulphur containing pollutants such as H_2S and SO_2. Especially in indoor environments the main crystalline corrosion product found on silver is Ag_2S[1, 2]. This is the reason why the interaction of silver with H_2S and SO_2 has been studied extensively, focusing on long term ex situ as well as some in-situ investigations. These conclude that silver seems to be most susceptible to H_2S in comparison to other inorganic corrosive gases[1, 2, 4, 5, 10, 12, 13, 21-25]. Less attention has been given to the influence of ozone on heritage silver corrosion, especially in combination with other

corrosive gases. Silver oxidation by ozone has been studied due to its importance in other fields of research, and it was shown that effects can be significant[7, 9, 14, 15, 26-28]. Furthermore, it was shown that the presence of ozone in a H_2S, SO_2 or CO_2 containing atmosphere increases silver corrosion rates tremendously[7, 9, 15, 28], although the exact reaction mechanisms have not been identified. Another important issue related to atmospheric corrosion is moisture. It has been shown that the corrosion rate on metals increases with increasing relative humidity (RH) in the surrounding atmosphere[1, 2, 15, 17, 29-32].

In this study a new set-up consisting of a customized eCell[20, 33] and a gas mixing unit[15] is presented to investigate in-situ the early stages of crystalline silver corrosion by time-lapse SR-XRD. First experiments have been performed by exposing highly pure silver to varying levels of RH, H_2S and O_3 in controlled atmospheres in order to see the early stages of crystalline corrosion product formation. The current study not only highlights some important facts related to the early stages of silver tarnishing but also shows the applicability of a new combined set-up for SR-XRD to study surface corrosion processes of metals in ambient atmosphere.

2. Experimental

2.1 Silver samples

For the experiments highly pure (99.9985%, Alfa Aesar®, USA) silver square coupons (25 x 25 mm^2, 2.0 mm thickness) were used. Before starting the weathering experiments the silver coupons were freshly abraded using SiC-paper with grits up to 4000 mesh, and surface finished by polishing with diamond paste (1 µm, Struers®, USA). The chosen polishing procedure gives uniform, reproducible surfaces. To remove remnants from the abrading and polishing procedure the samples were finally washed with 2-propanol in an ultrasonic bath for 10 min.

2.2 Gas mixing unit and environmental cell (eCell)

The gas mixing unit[15] used provides pure synthetic air which can be mixed with any RH content and corrosive gas. The gas concentrations and gas flow rate were controlled by high precision flowmeters (KROHNE®, Germany). The ozone was generated by an Ozonisator (Model Airmaster OMX 500, Topchem GmbH, Germany) and the gas concentration in the gas stream was monitored by gas sensors (Model AQL S500, Aeroqual Limited, New Zealand).

The environmental cell (eCell) is a unit which was created for in-situ XRD, XAS and XEOL measurements on a synchrotron beamline[33] and was already successfully applied to investigate chemical/electrochemical reactions in liquid environments[20, 33-35].

The gas mixing equipment and the eCell were combined for the very first time to perform in-situ and time resolved XRD measurements to observe crystalline surface changes on silver when exposed to corrosive gaseous atmospheres.

2.3 Synchrotron X-ray diffraction measurements

The in-situ SR-XRD measurements were performed at XMaS (beam line BM28, European Synchrotron Radiation Facility, Grenoble, France). X-rays at a wavelength of 0.15498 nm are directed to the sample surface at an angle of incidence of 10° with an estimated footprint of 1 mm x 200 µm. For the recording of 2D diffraction patterns a Mar CCD 165 detector (Mar USA, Inc., USA) was used. The acquisition time per image was 20 s. The axis of the CCD camera was oriented 45° to the incident X-ray beam. Data processing and treatment was done using esaProject 2013 software[35]. All data obtained were normalized to the beam monitor to compensate the beam decay. XRD patterns are given as intensity/counts vs. wave number Q where $Q=2\pi/d$ and d is the d-spacing). Q provides a wavelength-independent scale without the non-linearity of d-scale plotting. Identification of the silver corrosion products was done by comparing the XRD patterns with the JCPDS (Joint Committee on Powder Diffraction Standard Data) database (table 1), measured reference powders (Ag_2O, AgO, Ag_2S, Ag_2SO_4, Alfa Aesar®, USA) of silver corrosion products and literature[26, 27, 36-41].

Table 1: JCPDS References used to identify the formed corrosion products.

Compound	Crystal structure	JCPDS References
Ag	cubic	01-071-3762/01-089-3722
Ag_2O	cubic	00-041-1104/03-065-6811
AgO	monoclinic	00-051-0945/01-080-1269/00-043-1038
Ag_2O_3	orthorhombic	01-077-1289/00-040-0909
Ag_3O_4	monoclinic	01-084-1261/03-065-9750
Ag_2S	cubic/ monoclinic	01-071-0996/01-075-1061
Ag_2SO_3	monoclinic	01-070-1910/00-023-0644
Ag_2SO_4	orthorhombic/hexagonal	00-027-1403/00-040-1471

2.4 In-situ weathering experiments

The highly pure silver coupons were mounted in the eCell and subsequently exposed to different weathering atmospheres containing synthetic air containing 500 ppb O_3 and/or H_2S (500 ppb and 10 ppm) at 50% and 90% RH. The samples were weathered for periods of 12-24 h under ambient pressure and room temperature. During the weathering of the silver coupons in the eCell, SR-XRD patterns were recorded every 10 min.

3. Results and discussion

3.1 Silver exposed to Ozone and RH

A highly pure silver coupon was exposed for 24 h to a gaseous environment containing dry synthetic air, 500 ppb O_3 and 50% RH. SR-XRD diffractograms were recorded every 10 min to observe the growth of crystalline corrosion products on the silver surfaces. Figure 1 presents 3 diffractograms obtained after 0, 12, and 24 h of weathering. The diffractogram at time 0 h represents the unweathered sample showing the four characteristic reflections of pure polycrystalline silver (Ag 111, Ag 200, Ag 220, and Ag 311) indicated by the symbol * in Figure 1.

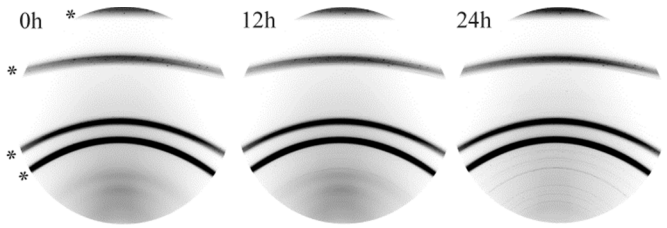

Fig.1 Raw SR-XRD images of a silver coupon exposed to synthetic air containing 500 ppb O_3 and 50% RH obtained after 0, 12, and 24 h of weathering.
Silver reflections are denoted by a *.

Over time additional reflections of silver corrosion products appear which are also visible in Figure 1. These new rings are diffuse and uniform indicating the growth of a polycrystalline layer with no preferred orientation. For better data representation, 1-D patterns were extracted from all 144 diffractograms obtained during weathering and collected in one plot to facilitate detailed comparison. In Figure 2 the time-lapse SR-XRD patterns plotted every 60 min (front to back) are shown.

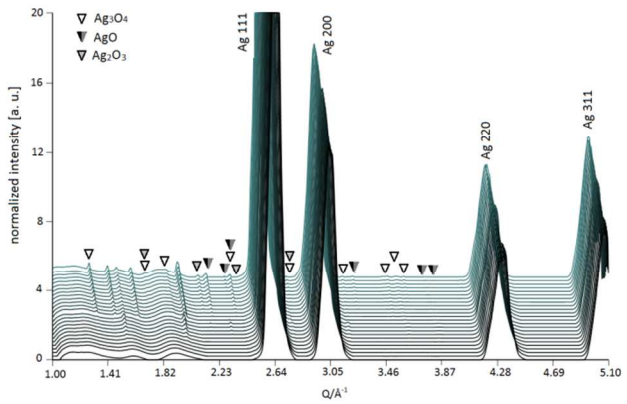

Fig.2 Waterfall plot of reprojected and normalized SR-XRD diffractograms of a silver coupon exposed to synthetic air containing 500 ppb O_3 and 50% RH for 24 h (60 min steps front to back). Pyramid labels indicate crystalline silver oxide species. The wave-like features at low wavenumbers are artifacts due to the geometric set-up.

The first detectable crystalline corrosion products on silver exposed to RH and O_3 are already visible as tiny reflections in Figure 2 after 3 h of weathering. These reflections could be attributed to cubic Ag_2O surface species. Further two new reflections appear after 4 h of weathering related to AgO ($Ag^{I}Ag^{III}O_2$ or $Ag_2O.Ag_2O_3$) corrosion products[39, 42, 43]. After 10 h of weathering single reflections start to split and further grow over time. This splitting is an indication of re-crystallization. Additionally, new reflections start to grow at this point of time - identified as mainly AgO, Ag_2O_3, and Ag_3O_4 crystalline species[39, 42, 44-47]. Furthermore, four reflections at low wavenumbers are visible which could not be identified. As those reflections also start to appear at the same time as the silver oxide crystalline species reflections it may be concluded that they are also related to silver oxides. Between 10 and 24 h the already visible reflections increase over time but no additional reflections appear until the end of the experiment. These results are a major hint that after 10 h of weathering the surface reactions occurring obviously change, leading to a change of crystalline structure of the silver corrosion products and therefore also indicating a transformation to different chemical surface species.

Figure 3 shows the integrated area of relevant reflections (calculated between two fixed wavenumbers for each reflection and baseline subtracted) related to the crystalline corrosion products (denoted as AgCorr) plotted against the combined reflection area of the pure silver reflections (denoted as Ag).

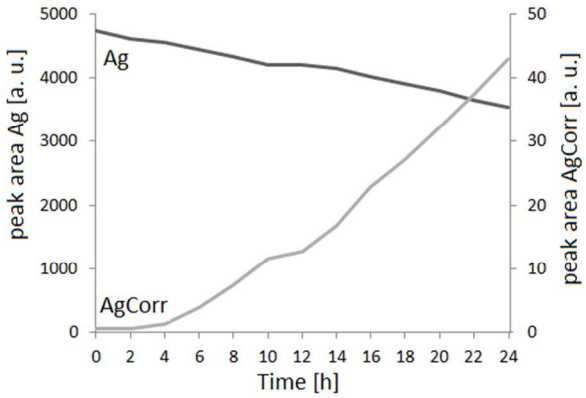

Fig.3 Reflection areas of SR-XRD patterns for silver (sum of the 4 Ag reflections labelled as Ag) and silver corrosion products (sum of all other reflections labelled as AgCorr) were calculated.

The functions have opposite trends which arise because the silver is being covered by the corrosion and its reflected intensity is absorbed in the superficial layer. The formation of the first crystalline corrosion products can already be observed after 2 h of weathering from the AgCorr line. This is also indicated by a nearly exponential growth of the AgCorr function for the weathering period in between 2 to 6 hours which changes afterwards to a linear behaviour. At the same time the Ag curve shows a more linear decline from the beginning. In both curves a change in slope is visible after 10h of weathering indicating a change of the corrosion rate. Between 10 and 12 h of weathering the corrosion proceeds linearly and more slowly, as shown by the flat gradients of the AgCorr and Ag curves. After 12 h of weathering the corrosion process proceeds linear and continuous until the end of the experiment.

In a second experiment a highly pure silver coupon was exposed to synthetic air, 500 ppb O_3 and an increased humidity of 90% RH to elucidate the influence of relative humidity to the

oxidation of silver. SR-XRD diffractograms were taken again every 10 min during weathering.

Figure 4 presents the time-lapse SR-XRD patterns plotted every 30 min. Besides the reflections for metallic polycrystalline silver two broad reflections are immediately visible after exposure (10min). The peak width here is indicative either of a very thin layer, in comparison to the last example, or very small crystallites which do not provide full coherent scattering, or the presence of disordered/amorphous phases[47]. As silver oxide has partially amorphous character[48, 49] a mixed amorphous-crystalline silver oxide species can be suspected. The reflection with a shoulder at low wavenumbers is attributed to Ag_2O and AgO species. The broad reflection at high wavenumbers seemingly consists of two reflections also related to Ag_2O and AgO. After 10 h of weathering a change in the recorded reflection patterns is visible. The reflection with a shoulder at low wavenumbers slightly broadens and is shifted to higher wavenumbers which could be an indication for Ag_3O_4 formation. The broad reflections at high wavenumbers - which consisted of two joined reflections during the first 10 h of weathering - separate to four reflections indicating the formation of Ag_2O_3 and Ag_3O_4 species.

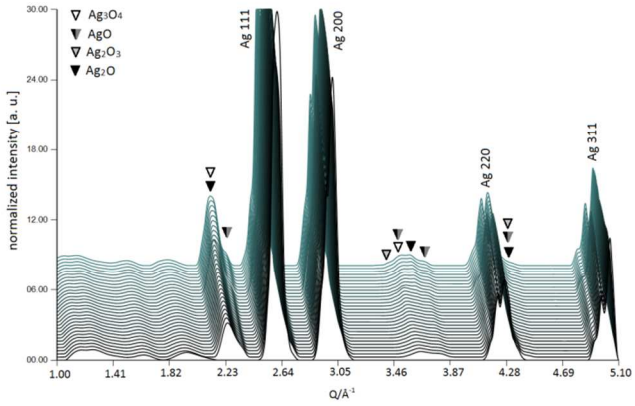

Fig.4 Waterfall plot of reprojected and normalized SR-XRD diffractograms of a silver coupon exposed to synthetic air containing 500 ppb O_3 and 90% RH for 18 h (30 min steps).

Also for this set of data the observed reflections (Figure 4) of the crystalline corrosion products and of pure silver were integrated and plotted against each other as shown in Figure 5.

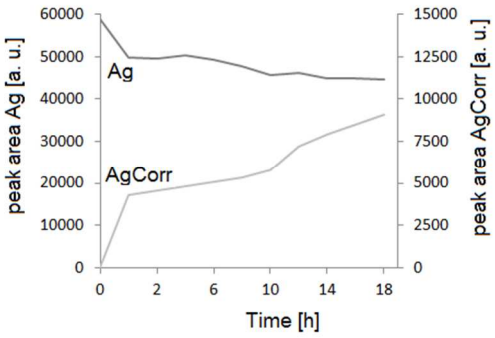

Fig.5 Peak areas of SR-XRD patterns for silver (sum of the 4 Ag reflections labelled as Ag) and silver corrosion products (sum of all other reflections labelled as AgCorr) were calculated.

Figure 5 shows the relation of the pure Ag peak areas to the sum of all other occurring peak areas. Again, we see inverse behaviour. Looking at the curve of AgCorr (sum of peak areas of corrosion products) the first crystalline corrosion products form immediately and are already detectable after 10 min. This fast corrosion process continues during the first hour. Between 1 and 10 h it proceeds linearly at a slower rate. In both curves a gradient change is visible after 10 h of weathering indicating a change of the corrosion process. Between 10 and 12 h the corrosion proceeds linearly but twice as fast as the hours before. From 12 h on the crystalline corrosion product formation slows down and proceeds linear and continuous until the end of the experiment.

Summing up the results obtained from a pure silver sample exposed to synthetic air and 500 ppb O_3 with 50 and 90% RH the following can be concluded. The sample exposed to 50% RH atmosphere shows the first detectable crystalline corrosion products after 3 h of weathering attributed to Ag_2O formation. With continuous exposure (4 h) the Ag_2O species is obviously oxidized to a AgO species which further increase with time. An important change of corrosion process is happening after 10 h of weathering governed by a change of crystalline structure and the appearance of new silver oxide crystalline species (AgO, Ag_2O_3, and Ag_3O_4). During this time (10-12 h) the growth rate of corrosion products is nearly zero (Figure 3, AgCorr curve). At the same time nearly no loss of base metal (Figure 3, Ag curve) is observed. After this point of time (12 h) the corrosion process proceeds linearly with no new crystalline species formed.

The sample exposed to higher RH (90%) immediately forms mixed amorphous-crystalline Ag_2O and AgO upon exposure (after 10 min). As already observed in the previous sample at 50% RH after 10 h of weathering a change of the corrosion process is visible indicated by the appearance of Ag_2O_3 and Ag_3O_4 species and the change of growth rate shown in Figure 5. In this case it can be stated that at higher RH content (90%) leads to a faster silver oxidation during the first hours and also favours the formation of mixed amorphous-crystalline Ag_2O and AgO surface species. The reason for this faster reaction at the beginning of the weathering might be an increased formation rate of OH-radicals at 90% RH by O_3 in the surface water film causing a subsequent accelerated silver oxide formation on the sample surface [9, 28, 50, 51]. After this first fast oxidation step the corrosion rate is decreased after 1 h and then proceeds slowly until the end of the experiment. This is the opposite for the sample in weathered in 50% RH where the corrosion rate is slower in the first 4 h of weathering and then sharply increases and proceeds at a high rate until the end of the experiment. This different behaviour might be explained by the formation of a dense oxide layer on the sample exposed to 90% RH which acts as an active diffusion barrier for reactive species

(from the bulk to the surface and vice versa) thus leading to a decreased long-term corrosion rate. On the other hand the oxide film formed on the sample exposed to 50% RH allows a further progression of the corrosion reactions.
Nevertheless, in both cases it could be shown that silver exposed to synthetic air and RH is highly susceptible to oxidize at already low concentrations of 500 ppb O_3 leading to a darkened/blackened sample surface appearance on all samples at the end of the weathering experiments.

3.2 Silver exposed to H_2S and RH

As silver is known to be highly susceptible to H_2S the experiments as described above were performed similarly, replacing O_3 by H_2S. A highly pure silver coupon was exposed to a gaseous environment containing synthetic air, 500 ppb H_2S and 50% RH. Again SR-XRD diffractograms were collected every 10 min during weathering. Figure 6 shows extracted patterns plotted every 30 min from front to back.

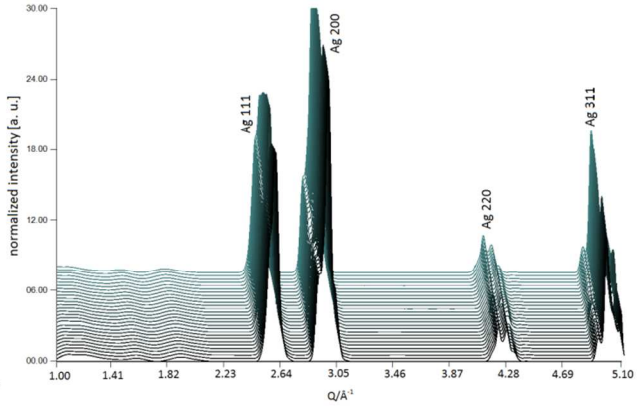

Fig.6 Waterfall plot of reprojected and normalized SR-XRD diffractograms of a silver coupon exposed to synthetic air containing 500 ppb H_2S and 50% RH for 18 h (30 min steps).

As shown in Figure 6 no obvious reflections are visible for the whole weathering time besides the ones for metallic silver. All patterns have been divided by the pattern for the sample at time 0h (reference).

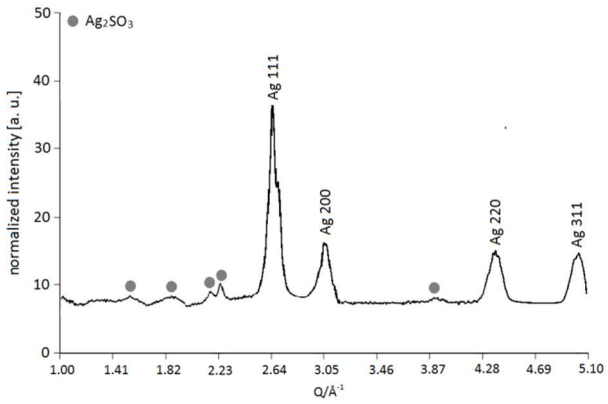

Fig.7 Reprojected SR-XRD diffractogram of a silver coupon exposed to synthetic air containing 500 ppb H_2S and 50% RH for 18 h. The pattern shown was obtained by dividing the pattern after 18 h by the pattern at time 0h (reference).

Figure 7 presents the pattern extracted from the diffractogram obtained after 18h of weathering also divided by the unweathered sample to better elucidate small changes occurring over time. Besides the reflections for metallic polycrystalline silver five small, broad reflections are visible which could be attributed to Ag_2SO_3 species. Those reflections are visible for the first time after 160 min (not presented in the figure) of weathering and grow very slowly until the end of the experiment. Furthermore, the sample did not show any visible signs of corrosion after the weathering process.
As these weathering conditions (synthetic air, 50% RH and 500 ppb H_2S) hardly lead to any detectable corrosion products, both the H_2S concentration and the RH were increased subsequently Therefore a new pure silver coupon was exposed to a 20 times higher H_2S concentration in 90% RH. Again SR-XRD diffractograms were taken every 10 min to identify crystalline corrosion product growth. Also under these aggressive weathering conditions nearly no crystalline corrosion products could be detected (not visible in the time-lapse waterfall plot). For this reason again the ratios of all diffractograms to the reference diffractogram were calculated.

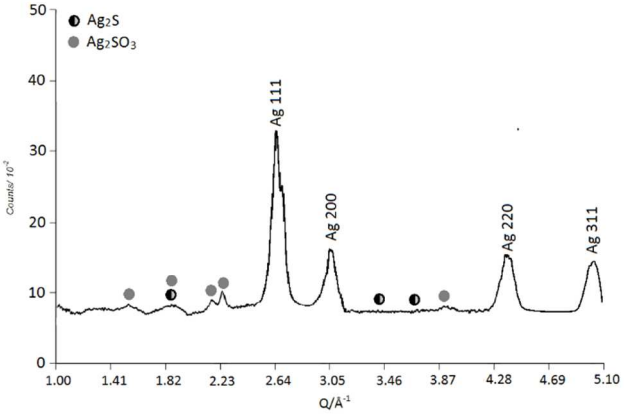

Fig.8 Reprojected and SR-XRD diffractogram of a silver coupon exposed to synthetic air containing 10 ppm H_2S and 90% RH for 12 h. The pattern shown was obtained by dividing the pattern after 18h by the pattern at time 0 h (reference).

In Figure 8 the reprojected SR-XRD diffractogram obtained after 12h of weathering divided by the reference (Ag coupon at time 0h) is shown. Mainly sharp reflections appeared over time which could be ascribed to Ag_2S, while the broad reflections were assigned to Ag_2SO_3. The first visible reflections appeared after 110 min of weathering assigned to both Ag_2S and Ag_2SO_3 species.

To clarify the influence of the ambient conditions on the growth rate of the corrosion products formed, the areas of the observed reflections of the corrosion products and pure silver were calculated and plotted against each other (Figure 9).

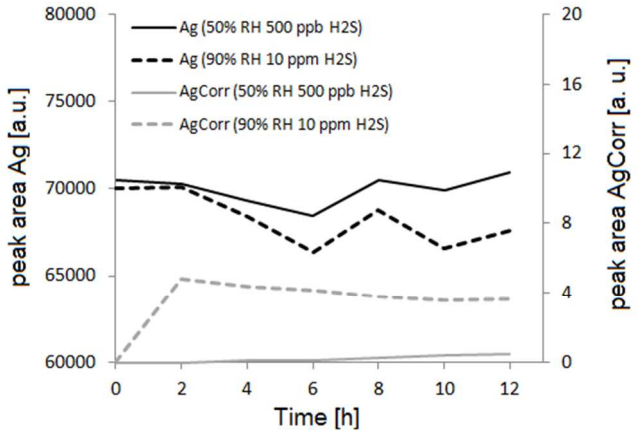

Fig.9 Comparison of peak areas of SR-XRD patterns for silver exposed to 50% RH and 500 ppb against silver exposed to 90% RH and 10 ppm H_2S.

For the silver sample exposed to 50% RH and 500 ppb H_2S an upward trend in the level of corrosion can be seen despite the small amplitude of the reflections. The calculated sum of peak areas for Ag reflections starts to decrease after 2 h of weathering indicating the covering of the silver by corrosion product. However, the lack of significant reflections in the XRD pattern indicated that this is principally amorphous.

Analysing at results from the silver sample exposed to 90% RH and 10 ppm H_2S, a relatively fast increase of the corrosion product formation rate can be observed for the first 2 h of weathering, followed by a sharp decrease at 2 h of weathering and a further very slow linear decrease until 12 h of weathering. The silver curve for this experiment shows nearly steady state behaviour for the first 2 h of weathering followed by a linear decrease until 6 h and then a rather unstable behaviour which needs to be investigated in more detail. In fact the Ag curves for both experiments show a similar trend after 6 hours with the Ag (50% RH 500 ppb H_2S) curve regaining its initial level at 12 hours. Given that the reflected silver intensity is controlled by the absorption in surface corrosion, one might interpret this as the appearance of metallic silver on top of the corrosion layer as well as a substrate, followed by reoxidation.

In summary it can be stated that silver forms only small amounts of crystalline corrosion product when exposed to 50% RH and 500 ppb H_2S over periods of 18 h. At higher RH (90%) and H_2S (10 ppm) silver is more prone to corrosion and forms crystalline Ag_2S and Ag_2SO_3 species.

As weathering conditions in this H_2S atmosphere did not lead to severe crystalline corrosion product formation O_3 was added in order to corrode the surface during the time frame of the synchrotron experiment.

3.3 Silver exposed to H_2S, Ozone and RH

Highly pure silver coupons were exposed to a gaseous environments containing synthetic air, 10 ppm H_2S and 90% RH. After 12 h of weathering, additionally 500 ppb O_3 was added to the gas stream to elucidate the influence of a strong oxidizing agent on other corrosive atmospheres. SR-XRD diffractograms were taken every 10min for a total weathering time of 24 h as shown in Figure 10.

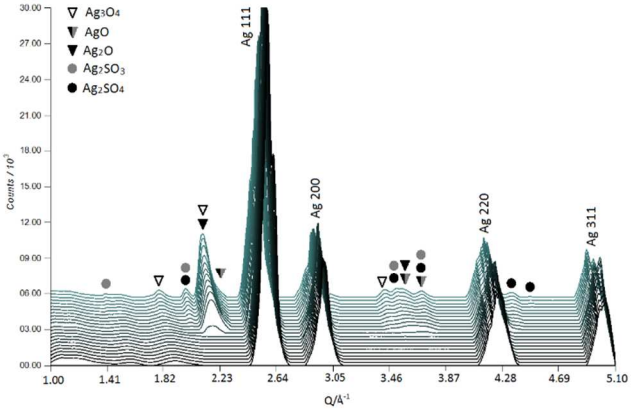

Fig.10 Waterfall plot of reprojected and normalized SR-XRD diffractograms of a silver coupon exposed to synthetic air containing 10 ppm H_2S and 90% RH for 12 h (30 min steps). After 12 h 500 ppb O_3 was additionally added to this atmosphere.

Already after 30 min of O_3 addition to the H_2S containing atmosphere (12 h and 30 min total weathering time) two additional reflections appear, attributed to silver-oxide species. After 1 h two further reflections at low wavenumbers appear, due to Ag_2SO_3 and Ag_2SO_4 crystalline species. Furthermore, the broad reflection at higher wavenumbers starts to split into 4 separate reflections attributed to AgO, Ag_3O_4, Ag_2SO_3 and Ag_2SO_4 species. The fastest growth rate over time is shown by Ag_2O and AgO species. Regarding the overall corrosion product formation, the contribution of sulfate compounds is minor and silver sulfide species could not be detected at all at the point of O_3 addition.

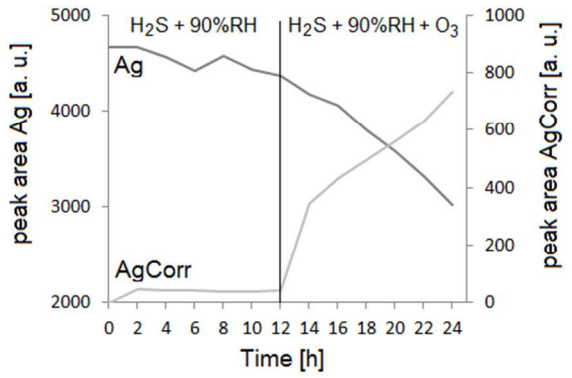

Fig.11 Peak areas of SR-XRD patterns for silver exposed to 10 ppm H_2S and 90% RH. After 12 h 500 ppb O_3 was added to this atmosphere for another 12 h. Sum of the 4 Ag reflections labelled as Ag and sum of all other reflections labelled as AgCorr.

Figure 11 presents the corrosion growth behaviour (peak areas of obtained SR-XRD reflections) of a silver coupon exposed to 10 ppm H_2S and 90% RH. After 12 h 500 ppb O_3 was added to this atmosphere for additionally 12 h.

It is immediately obvious that the addition of O_3 to the H_2S-containing atmosphere causes an increased formation of corrosion products. After O_3 addition the curve of AgCorr formation exhibits approximately parabolic growth for the first 22 h of weathering which suggests diffusion-controlled oxidation governed by a Fickian transport mechanism[52]. Obviously the minor formation of corrosion products formed during H_2S exposure (0-12 h) leads to an immediate overtaking by O_3 influenced corrosion. As O_3 is known to react with H_2S to form SO_2 in a gaseous environment not only silver-oxides are formed upon O_3 addition but also silver-sulfites and –sulfates.

3.4 Considerations related to SR-XRD measurements in the beam-line ambient atmosphere

Independent of the weathering conditions, during the time-lapse measurements a concentration of 20-70 ppb O_3 was measured. This O_3 is produced by the x-ray beam in contact with oxygen containing atmospheres. It is highly probable that this O_3 concentration influences the corrosion/surface reaction process during the measurements and should be taken into account. In this case the experiments performed in RH and H_2S atmosphere have probably been influenced by the O_3 caused by the beam. This could explain the preferential formation of Ag_2SO_3 and Ag_2SO_4 species in those experiments rather than the expected Ag_2S. For the samples which were exposed to O_3 (500 ppb) the additional O_3 produced by the beam will not significantly change the corrosion mechanism but it should be taken into account that the O_3 concentration during measurements was raised by 4-14%.

Another issue related to the SR-XRD measurements is of the effect of the experiment on the surface spot to be analysed. Due to the high energy of the excitation beam an influence on the surface reactions has to be considered. For the samples exposed to O_3 and RH which showed a black corrosion layer, a visible surface mark could be observed (a brighter, line shaped area in the blackened surface) caused by the beam. This is due to the possible influence of surface changes (chemistry) caused by the method in certain conditions and needs further clarification. Further detailed and systematic investigations can reveal these measurement caused/induced surface artefacts.

Conclusions

This work presents the first documented use of in-situ time-lapse SR-XRD to investigate early stages of atmospheric corrosion on metals. Furthermore, the applicability of the eCell to investigate metal surfaces in controlled gaseous environments in-situ by time resolved SR-XRD could be demonstrated.

Following those time-resolved in-situ results it could be shown that crystalline corrosion products on silver exposed to 500 ppb O_3 and 50% RH start to form already after 3 h of weathering, leading to a blackened (tarnished) silver surface after 24 h of weathering. At 90% RH in O_3 atmosphere silver oxidation starts immediately but more mixed oxide species (crystalline-amorphous) are formed. It could also be shown that silver is less susceptible to H_2S and SO_2 compared to O_3. In both cases the O_3 and H_2S (500 ppb) concentrations of the experiments are not so much higher than the measured O_3 and H_2S concentrations in city atmospheres. In combination with other gases related to silver tarnishing the corrosive potential of O_3 should not be underestimated.

Acknowledgements

The authors are grateful to XMaS the UK CRG at the ESRF for funding the beam time used in this paper. XMaS is funded as a Mid-Range Facility by the Engineering and Physical Sciences Research Council (EPSRC) UK. The authors would like to acknowledge the Warwick Physics department and Bijzonder Onderzoekfonds at Universiteit Gent for studentship funding of RG. Furthermore, the authors would like to thank Derrick Richards and Adrian Lovejoy for the construction of the eCell and related electronics. The eCell was developed using funding from The Paul Instrument Fund of the Royal Society and EVA Surface Analysis, UK. esaProject and the eCell design are copyright 2013 Dowsett and Adriaens, and made available by EVA Surface Analysis. Also support from the Fund for Scientific Research – Flanders (FWO) is gratefully acknowledged.

Notes and references

[a] Institute of Science and Technology in Art, Academy of Fine Arts Vienna, 1010 Vienna, Schillerplatz 3, Austria
[b] Electrochemistry and Surface Analysis Group, Department of Analytical Chemistry, Ghent University, Belgium

[c] Analytical Science Projects, Department of Physics, University of Warwick, UK
[d] XMaS (BM28), BP 220, 38043 Grenoble, France

1. T. E. Graedel, *J. Electrochem. Soc.*, 1992, 139, 1963-1970.
2. C. Leygraf and T. E. Graedel, *Atmospheric Corrosion*, John Wiley & Sons, New York, 2000.
3. T. E. Graedel, D. T. Hawkins and L. D. Claxton, *Atmospheric chemical compounds: sources, occurrence and bioassay*, Academic Press, Orlando, 1986.
4. J. P. Franey, G. W. Kammlott and T. E. Graedel, *Corros. Sci.*, 1985, 25, 133-143.
5. H. Kim, *Mater. Corros.* 2003, 54, 243-250.
6. D. W. Rice, P. Peterson, E. B. Rigby, P. B. P. Phipps, P. J. Cappell and R. Tremoureux, *J. Electrochem. Soc.*, 1981, 128, 275-284.
7. D. Liang, H. C. Allen, G. S. Frankel, Z. Y. Chen, R. G. Kelly, Y. Wu and B. E. Wyslouzil, *J. Electrochem. Soc.*, 2010, 157, C146-C156.
8. D. Persson and C. leygraf, *J. Electrochem. Soc.*, 1993, 140, 4.
9. Z. Y. Chen, D. Liang, G. Ma, G. S. Frankel, H. C. Allen and R. G. Kelly, *Corros. Eng., Sci. Technol*, 2010, 45, 169-180.
10. T. E. Graedel, J. P. Franey, G. J. Gualtieri, G. W. Kammlott and D. L. Malm, *Corros. Sci.*, 1985, 25, 1163-1180.
11. K. Hallett, D. Thickett, D. S. McPhail and R. J. Chater, *Appl. Surf. Sci.*, 2003, 203-204, 789-792.
12. C. Kleber, R. Wiesinger, J. Schnöller, U. Hilfrich, H. Hutter and M. Schreiner, *Corros. Sci.*, 2008, 50, 1112-1121.
13. D. Pope, H. R. Gibbens and R. L. Moss, *Corros. Sci.*, 1968, 8, 883-887.
14. G. I. N. Waterhouse, G. A. Bowmaker and J. B. Metson, *Appl. Surf. Sci.*, 2001, 183, 191-204.
15. R. Wiesinger, M. Schreiner and C. Kleber, *Appl. Surf. Sci.*, 2010, 256, 2735-2741.
16. C. Kleber, R. Wiesinger, J. Schnöller, U. Hilfrich, H. Hutter and M. Schreiner, *Corros. Sci.*, 2008, 50, 1112-1121.
17. T. E. Graedel, *Corros. Sci.*, 1996, 38, 2153–2180.
18. N. Birbilis, K. Meyer, B. C. Muddle and S. P. Lynch, *Corros. Sci.*, 2009, 51, 1569-1572.
19. K. Leyssens, A. Adriaens, M. G. Dowsett, B. Schotte, I. Oloff, E. Pantos, A. M. T. Bell and S. P. Thompson, *Electrochemistry Communications*, 2005, 7, 1265-1270.
20. R. Grayburn, M. Dowsett, M. De Keersmaecker, E. Westenbrink, J. A. Covington, J. B. Crawford, M. Hand, D. Walker, P. A. Thomas, D. Banerjee and A. Adriaens, *Corros. Sci.*, 2014, 82, 280-289.
21. D. A. Outka and R. J. Madix, *Surf. Sci.*, 1984, 137, 242-260.
22. W. S. Lassiter, *J. Phys. Chem.*, 1972, 76, 1289-1292.
23. M. Watanabe, H. Ando, T. Handa, T. Ichino and N. Kuwaki, *Zairyo-to-Kankyo*, 2007, 56, 10-15.
24. V. Costa, *Reviews in Conservation*, 2001, 2, 19-21.
25. J. Schnoller, R. Wiesinger, C. Kleber, U. Hilfrich, M. Schreiner and H. Hutter, *Anal Bioanal Chem*, 2008, 390, 1543-1549.
26. G. I. N. Waterhouse, G. A. Bowmaker and J. B. Metson, *Surf. Interface Anal.*, 2002, 33, 401-409.
27. R. O. Suzuki, T. Ogawa and K. Ono, *J. Am. Ceram. Soc.*, 1999, 82, 2033-2038.
28. R. Wiesinger, I. Martina, C. Kleber and M. Schreiner, *Corros. Sci.*, 2013, 77, 69-76.
29. P. B. P. Phipps and D. W. Rice, *Corrosion Chemistry*, 1979, 89, 235-261.
30. M. Salmeron, H. Bluhm, N. Tatarkhanov, G. Ketteler, T. K. Shimizu, A. Mugarza, X. Y. Deng, T. Herranz, S. Yamamoto and A. Nilsson, *Faraday Discuss.*, 2009, 141, 221-229.
31. W. Stumm, *Chemistry of the Solid Water Interface*, John Wiley & Sons, New York, 1992.
32. P. B. P. Phipps and D. W. Rice, *The Chemistry of Corrosion*, ACS Publication, Washington D.C., 1979.
33. M. Dowsett and A. Adriaens, *Anal. Chem.*, 2006, 78, 3360-3365.
34. M. Dowsett and A. Adriaens, *Acc. Chem. Res.*, 2009, 43, 927-935.
35. A. Adriaens, M. Dowsett, K. Leyssens and B. Van Gasse, *Anal Bioanal Chem*, 2007, 387, 861-868.
36. M. F. Al-Kuhaili, *J. Phys. D: Appl. Phys.*, 2007, 40, 2847-2853.
37. N. R. C. Raju, K. Jagadeesh Kumar and A. Subrahmanyam, *J. Phys. D: Appl. Phys.*, 2009, 42, 135411-135417.
38. M. N. V. Ramesh, Y. Sundarayya and C. S. Sunandana, *Mod. Phys. Lett. B*, 2007, 21, 1933-1944.
39. G. I. N. Waterhouse, G. A. Bowmaker and J. B. Metson, *Phys. Chem. Chem. Phys.*, 2001, 3, 3838-3845.
40. U. K. Barik, S. Srinivasan, C. L. Nagendra and A. Subrahmanyam, *Thin Solid Films*, 2003, 429, 129-134.
41. S. Ando, T. Hioki, T. Yamada, N. Watanabe and A. Higashitani, *J. Mater. Sci.*, 2011.
42. D. Tudela, *J. Chem. Educ.*, 2008, 85, 863-865.
43. F. Hong-Liang, G. Xiao-Yong, Z. Zeng-Yuan and M. Jiao-Min, *J. Korean Phys. Soc.*, 2010, 56, 1176-1179.
44. B. Standke and M. Jansen, *Angew. Chem.*, 1985, 24, 118-119.
45. G. Xiaoyong, *J. Korean Phys. Soc.*, 2010, 56, 1176.
46. G. I. N. Waterhouse, J. B. Metson and G. A. Bowmaker, *Polyhedron*, 2007, 26, 3310-3322.
47. T. C. Kaspar, T. Droubay, S. A. Chambers and P. S. Bagus, *J. Phys. Chem. C*, 2010, 114, 21562-21571.
48. W. Wei, X. Mao, L. A. Ortiz and D. R. Sadoway, *Journal of Materials Chemistry*, 2011, 21, 432.
49. S. Günther, S. Böcklein, R. Reichelt, J. Wintterlin, B. A, T. Menteş, M. Niño and A. Locatelli, *ChemPhysChem*, 2010, 11, 1125-1532.
50. X. Bao, M. Muhler, B. Pettinger, R. Schlögl and G. Ertl, *Catal. Lett.*, 1993, 22, 215-225.
51. X. Bao, M. Muhler, B. Pettinger, Y. Uchida, G. Lehmpfuhl, R. Schlögl and G. Ertl, *Catal. Lett.*, 1995, 32, 171-183.
52. A. d. Rooij, *ESA J.*, 1989, 13, 363-382.